Tellus (2001), 53A, 146–167
Printed in UK. All rights reserved

TELLUS
ISSN 0280–6495

Ideal shocks in 2-layer flow

Part II: Under a passive layer

By QINGFANG JIANG and RONALD B. SMITH*, *Department of Geology and Geophysics, Yale University, New Haven, Connecticut 06520-8109, USA*

(Manuscript received 17 May 1999; in final form 2 October 2000)

ABSTRACT

In this second part of the study, ideal shock theory in two-layer stratified flow is extended to include a third passive layer (i.e., a two and a half layer system). With the presence of a passive layer, two linear wave modes and "viscous tail modes" exist, complicating the solubility conditions and uniqueness proofs for two layer shocks. It is found however, that shocks can be unambiguously classified as external or internal based on the states of criticality that they connect. The steepening condition, while still necessary, provides a less restrictive constraint than it did with a rigid lid. Thus, we have to rely more on solutions to the full viscous shock equations to establish shock existence. The detailed structure, momentum exchange, and Bernoulli loss in a viscous shock are examined using an analytical weak shock solution and a set of numerical solutions for shocks with finite amplitudes. A shock regime diagram (F_1 by F_2) is constructed based on the numerical integration of the full viscous shock equations. For strong external jumps, a cusp region (i.e., in the sense of catastrophe theory) is identified on the regime diagram. For pre-shock states within the cusp, three end states are possible and two of these are realizable. The cusp has several physical implications. It indicates that an equal distribution of dissipation between the two layers in shocks is mathematically possible but physically inaccessible. It also allows hysteresis in time varying flows, and promotes the occurrence of double shocks (i.e., closely spaced shocks of different character). The results are compared with classical shock solutions and a set of time dependent numerical experiments.

1. Introduction

Hydraulic jumps or "shocks" are commonly seen in layer-like density-stratified flows in a gravity field. A theoretical understanding of jumps has been sought by meteorologists, oceanographers and engineers. Previous two-layer shock theories can be classified into three categories. One category was built on an assumed formula for momentum exchange between two layers (Yih and Guha, 1955, hereafter YG55). Yih and Guha assumed that interfacial mixing was negligible and that the momentum exchange due to pressure on the sloping interface can be expressed as the product of a 'mean' pressure and lower layer depth change. The YG theory has a nice form, and gives reasonable results in some cases, but it contains a number of physical inconsistencies such as a prediction of energy gain in the contracting layer (Baines, 1995).

Another category of theory was built on an assumed energy loss across the jump such as Chu and Baddour (1977), Wood and Simpson (1984), Armi (1986), Armi and Williams (1993), and Klemp et al. (1997). These theories are simple to evaluate and depending on which energy loss assumption is used, they compare well with various types of experimental data. A problem with this type of theory is that it is unclear how to

* Corresponding author.
e-mail: ronald.smith@yale.edu

apply them to new situations, without guidance from experimental data or numerical simulations. For example, if the assumption of energy conservation in one expanding layer is selected, how does one handle situations where both layers expand? It would be better to have a theory that would predict energy loss, instead of assuming it.

The third category of two-layer shock theory was developed in part I (i.e., Jiang and Smith, 2001). In this new approach, a set of viscous model equations are formulated with three a priori assumptions: (a) no mixing of mass or momentum between layers; (b) nearly hydrostatic flow in the shocks; (c) dissipation occurs according to a viscous model. Shocks which satisfy these assumptions are called "ideal" in our terminology. With the assumption of a rigid lid, the analysis in Part I showed that these model equations could be used to establish shock existence and uniqueness and to predict the energy loss in each layer. While these predictions do not agree with some datasets, (e.g., those cases where assumption (a) is invalid; see Klemp et al., 1997) the general method could be extended with a less restrictive mixing formulation. A feature of the new theory is that its assumptions are consistent with earlier theoretical treatments of shocks in complex flows such as Houghton and Isaacson (1968), Schär and Smith (1993, hereafter SS93), and Smith and Smith (1995, hereafter SS95) and thus it can be used to diagnose those results.

In this paper, we seek to extend the "ideal" shock theory from the rigid lid case to the case with a passive layer aloft. This modest generalization is quite challenging as the second interface introduces a second wave mode, a second wave speed and a second Froude Number. In spite of these difficulties, we are able to derive shock existence and uniqueness conditions, classify all shocks, display a shock regime diagram and obtain an analytical solution for weak shocks.

The outline of this paper is as follows. The governing equations for a two and a half layer hydrostatic flow and the inviscid linear wave modes are discussed in Section 2. A viscous shock theory is developed in Section 3. It includes formulation, weak shock solutions and a discussion of viscous tail modes. A shock regime diagram is constructed in Section 4. A comparison among viscous shock solutions, YG shock solutions and shallow water simulations is given in Section 5. A summary is given in Section 6.

2. The two-and-a-half layer flow system

2.1. *Hydrostatic equations for a two and a half layer flow*

For a two-layer density stratified fluid under a third passive layer (Fig. 1), the hydrostatic equations take on the form (Houghton, 1964):

$$\frac{D\boldsymbol{V}_1}{Dt} + g\frac{\rho_1-\rho_3}{\rho_1}\nabla(h_1+h) + g\frac{\rho_2-\rho_3}{\rho_1}\nabla h_2 = 0, \tag{1}$$

$$\frac{D\boldsymbol{V}_2}{Dt} + g\frac{\rho_2-\rho_3}{\rho_2}\nabla(h_1+h_2+h) = 0, \tag{2}$$

$$\frac{Dh_i}{Dt} + h_i\nabla\cdot\boldsymbol{V}_i = 0, \tag{3}$$

where $\boldsymbol{V}_i = (u_i, v_i)$ is the horizontal velocity, g is the gravity, h_i are layer depths, and $h(x, y)$ refers to the elevation of the bottom topography, ρ_i are fluid densities, and the index $i = 1, 2, 3$ refers to the lower layer, the upper layer, and a third passive layer respectively. The uppermost fluid layer is assumed to be either indefinitely deep or with zero velocity, preventing it from supporting a pressure gradient, i.e., it is passive. In the Boussinesq limit, i.e., assuming the density difference is small, i.e.

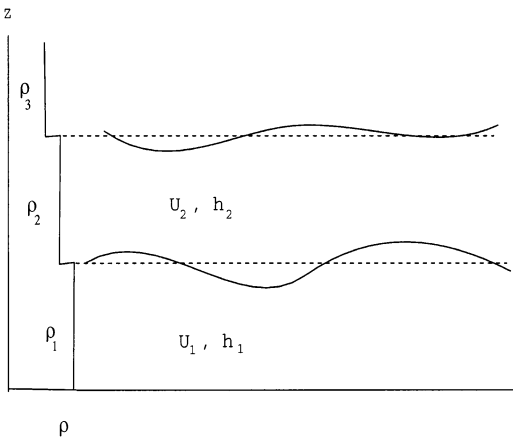

Fig. 1. Definition sketch of two and a half layer flow: ρ_1, ρ_2, ρ_3 are densities; h_1 and h_2 are flow depths; U_1 and U_2 are flow speeds. The third layer is passive.

$(\rho_1 - \rho_3) \ll \rho_1$, the above equations can be written in a more compact form:

$$\frac{D\boldsymbol{V}_1}{Dt} + g'(h + h_1 + rh_2) = 0, \tag{4}$$

$$\frac{D\boldsymbol{V}_2}{Dt} + rg'\nabla(h_1 + h_2 + h) = 0, \tag{5}$$

$$\frac{Dh_i}{Dt} + h_i\nabla \cdot \boldsymbol{V}_i = 0, \tag{6}$$

where $g' = g(\rho_1 - \rho_3)/\rho_1$ is the reduced gravity and $r = (\rho_2 - \rho_3)/(\rho_1 - \rho_3)$ is the density step ratio.

It is interesting to compare eqs. (4–6) to the equations governing two layer hydrostatic Boussinesq flow under a free surface. With $\rho_3 = 0$ and $\rho_2/\rho_1 \sim 1$ in eqs. (1) and (2), the continuity equations and the momentum equations can be written in nondimensional form as

$$\frac{D\boldsymbol{V}_1}{Dt} + g'\nabla(h + h_1 + rh_2) = 0, \tag{7}$$

$$\frac{D\boldsymbol{V}_2}{Dt} + g'\nabla(h_1 + h_2 + h) = 0, \tag{8}$$

$$\frac{Dh_i}{Dt} + h_i\nabla \cdot \boldsymbol{V}_i = 0, \tag{9}$$

where $r = \rho_2/\rho_1$ and $g' = g(1 - \rho_2/\rho_1)$. Notice that eqs. (4) and (6) are identical with (7) and (9). The only difference between eqs. (5) and (2) is that there is an extra r in eq. (5). Therefore, in the Boussinesq limit, two layer flow and two and a half layer flow have the same solutions if only the upper layer velocity $\boldsymbol{V}_2$ in a two layer flow is replaced by $\boldsymbol{V}_2/r$.

Hence, the results and conclusions in this study can be directly applied to both two layer Boussinesq flow under a third passive layer and two layer Boussinesq flow with no medium above. This correspondence would fail if mixing across the upper interface occurred.

2.2 *Linear waves*

For a two layer Boussinesq flow under a third passive layer, using eqs. (4–6), the linearized one-dimensional governing equations can be written as

$$\left(\frac{\partial}{\partial t} + U_1\frac{\partial}{\partial x}\right)u_1 + g'(\eta_1 + r\eta_2) = 0, \tag{10}$$

$$\left(\frac{\partial}{\partial t} + U_2\frac{\partial}{\partial x}\right)u_2 + rg'(\eta_1 + \eta_2) = 0, \tag{11}$$

$$\left(\frac{\partial}{\partial t} + U_1\frac{\partial}{\partial x}\right)\eta_1 + H_1\frac{\partial u_1}{\partial x} = 0, \tag{12}$$

$$\left(\frac{\partial}{\partial t} + U_2\frac{\partial}{\partial x}\right)\eta_2 + H_2\frac{\partial u_2}{\partial x} = 0. \tag{13}$$

The basic state is defined by flow speed U_1 (in the lower layer) and U_2 (in the upper layer), and flow depth H_1 (of the lower layer) and H_2 (of the upper layer), and density difference ratio r. u_1 and u_2 are small perturbations in velocity, and η_1 and η_2 are small displacements of the lower and upper interface.

Defining $\alpha = \eta_2/\eta_1$, from eqs. (10–13), we obtain:

$$\alpha = \frac{rg'H_2}{(c + U_2)^2 - rg'H_2} = \frac{(c + U_1)^2 - g'H_1}{rg'H_1}. \tag{14}$$

Using the normal mode method, the dispersion relation can be obtained:

$$\left(\frac{(U_1 - c)^2}{g'H_1} - 1\right)\left(\frac{(U_2 - c)^2}{g'H_2} - r\right) - r^2 = 0, \tag{15}$$

where c is the complex phase speed of gravity waves.

Eq. (15) admits 4 real roots for c, corresponding to two wave modes. Considering the existence of the third layer, both modes are internal. For convenience, in this article, the faster wave mode is referred to as the external mode, and the slower wave mode is termed the internal mode.

Letting $c = 0$, we obtain the critical condition to have one of the wave modes be stationary relative to the laboratory coordinate (Benton, 1954):

$$(F_1^2 - 1)(F_2^2 - r) - r^2 = 0, \tag{16}$$

where $F_1 = U_1/\sqrt{g'H_1}$ and $F_2 = U_2/\sqrt{g'H_2}$ are Froude number for the lower and upper layer.

On a Froude number diagram, eq. (16) describes a two branch curve (Fig. 2). The lower left branch corresponds to a stationary internal wave mode, and the upper-right branch corresponds to a stationary external wave mode. These two branches

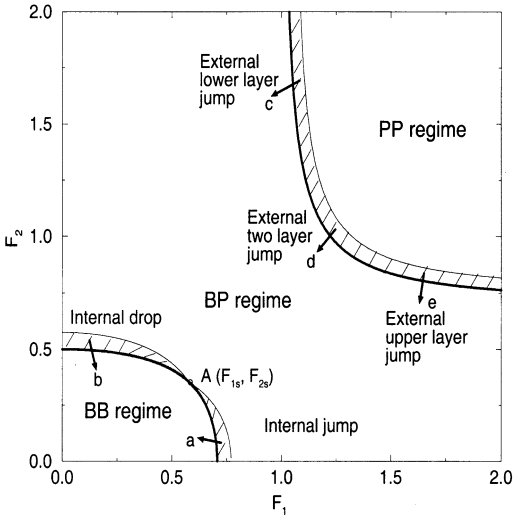

Fig. 2. Weak shock solutions. The bold curves represent the critical condition (1), which divides the diagram into three states of critcality, namely, BB regime, BP regime, and PP regime. The regions where weak shock solutions are valid are shaded. Point A is the singular point (F_{1s}, F_{2s}). Possible shocks are schematically shown as arrows pointing from allowable pre-shock states to possible post-shock states. 5 types of shocks are shown.

divide the diagram into three states of criticality: the BB, BP, and PP regimes. The notations can be found in Table 1. The symbols B and P are taken from the terms suBcritical and suPercritical. For example, in BP, the flow is subcritical to one mode and supercritical to the other. From (14), for a stationary internal wave $\alpha < 0$, and for a stationary external wave $\alpha > 0$.

3. Viscous shock theory

3.1. Formulation

3.1.1. Momentum balance in a two-layer shock. For a two layer Boussinesq flow under a passive third layer, the steady momentum equations in a viscous shock take the following form (SS93, SS95 and JS00b):

$$\frac{\mathrm{d}M_1}{\mathrm{d}x} = f_{1x} + (P_2 + P_3)\frac{\mathrm{d}h_1}{\mathrm{d}x}, \tag{17}$$

$$\frac{\mathrm{d}M_2}{\mathrm{d}x} = f_{2x} - (P_2 + P_3)\frac{\mathrm{d}h_1}{\mathrm{d}x} + P_3\left(\frac{\mathrm{d}h_1}{\mathrm{d}x} + \frac{\mathrm{d}h_2}{\mathrm{d}x}\right), \tag{18}$$

where M_1 is the generalized momentum in the lower layer,

$$M_1 = \rho_1\frac{Q_1^2}{h_1} + \frac{1}{2}gh_1 \times (\rho_1 h_1 + 2\rho_2 h_2 + 2\rho_3 D - 2\rho_3 h_1 - 2\rho_3 h_2). \tag{19}$$

M_2 is the generalized momentum in the upper layer,

$$M_2 = \rho_2\frac{Q_2^2}{h_2} + \frac{1}{2}gh_2 \times (\rho_2 h_2 + 2\rho_3 D - 2\rho_3 h_1 - 2\rho_3 h_2). \tag{20}$$

The other variables are as follows. $P_2 = \rho_2 g h_2$ is the hydrostatic pressure on the lower interface, $P_3 = \rho_3 g D - \rho_3 g h_1 - \rho_3 g h_2$ is the hydrostatic pressure on the upper interface, (h_1, h_2) are the flow depths of the lower and upper layers, D is the height of an arbitrary reference level within the passive layer, (ρ_1, ρ_2, ρ_3) are densities of the first, second, and third layer, $Q_1 = U_1 h_1$ and $Q_2 = U_2 h_2$ are mass fluxes in the lower and upper layer, and f_{1x} and f_{2x} are viscous forces in flux form.

According to SS95,

$$f_{1x} = \frac{\partial}{\partial \mathrm{x}}\left[\nu_1 h_1\left(\frac{Q_1}{h_1}\right)_x\right], \tag{21}$$

$$f_{2x} = \frac{\partial}{\partial \mathrm{x}}\left[\nu_2 h_2\left(\frac{Q_2}{h_2}\right)_x\right], \tag{22}$$

where ν_1 and ν_2 are viscous coefficients in the lower and upper layer, respectively. For

Table 1. *Shock regimes and eigenvalues*

BB	subcritical to both internal and external modes	$\lambda_{\mathrm{ext}} < \lambda_{\mathrm{int}} < 0$
BP	internally supercritical and externally subcritical (-j = jump, -d = drop, -n = no shock)	$\lambda_{\mathrm{ext}} < 0$ and $\lambda_{\mathrm{int}} > 0$
PP	supercritical to both internal and external modes	$\lambda_{\mathrm{int}} > \lambda_{\mathrm{ext}} > 0$
	(-1 = unique conjugate state, -3 = three conjugate states, -∞ = infinity of conjugate states)	

Newtonian fluids, v_1 and v_2 are constants. The different behavior of Newtonian and Non-Newtonian fluids and its effect on the Bernoulli change was addressed in Part I. In this part, we confine the analysis to Newtonian fluids and further assume that $v_1 = v_2 = v$.

3.1.2. TM conservation across a two-layer shock. Noticing that the viscous terms are in flux form, integrating (17) and (18) across the shock gives expressions relating the upstream and downstream (primed) variables:

$$M_1 = M_1' + M_{12} + \rho_2 g D(h_1' - h_1) - \tfrac{1}{2}\rho_2 g(h_1'^2 - h_1^2), \tag{23}$$

$$M_2 = M_2' - M_{12} + \rho_3 g D(h_2' - h_2) \tfrac{1}{2}\rho_3 g(h_2'^2 - h_2^2) - \rho_3 g(h_1' h_2' - h_1 h_2), \tag{24}$$

where

$$M_{12} = (\rho_2 - \rho_3) g \int_u^d h_2 \, \mathrm{d}h_1. \tag{25}$$

One can cancel out M_{12} by adding eqs. (23) and (24). Using Boussinesq approximation, we obtain:

$$\frac{Q_1^2}{h_1} + \frac{Q_2^2}{h_2} + \frac{1}{2} g'(h_1^2 + r h_2^2) + r g' h_1 h_2 = \frac{Q_1^2}{h_1'} + \frac{Q_2^2}{h_2'} + \frac{1}{2} g'(h_1'^2 + r h_2') + r g' h_1' h_2', \tag{26}$$

where $g' = g(\rho_1 - \rho_3)/\rho_1$ is the reduced gravity, and $r = (\rho_1 - \rho_2)/(\rho_1 - \rho_3)$ is the density step ratio.

Based on eq. (26), one can define a nondimensional total momentum TM

$$\mathrm{TM} = \frac{Q_1^2}{h_1} + \frac{Q_2^2}{h_2} + \frac{1}{2}(h_1^2 + r h_2^2) + r h_1 h_2, \tag{27}$$

where (h_1, h_2) are scaled with the lower layer upstream depth h_{1a}, TM is scaled with $g' h_{1a}^2$, and (Q_1, Q_2) are scaled with $g'^{1/2} h_{1a}^{3/2}$. The quantity TM is a conserved quantity across a shock in a two and a half layer flow. Potential post-shock states must have the same TM value as the pre-shock state (Benton, 1954).

3.1.3. Governing equations. Substituting (21) and (22) into eqs. (17) and (18), we obtain

$$\left(-\frac{Q_1^2}{h_1^2} + g' h_1\right) h_{1x} + r g' h_1 h_{2x} = v \frac{\partial}{\partial x}\left[h_1 \left(\frac{Q_1}{h_1}\right)_x\right], \tag{28}$$

$$r g' h_2 h_{1x} + \left(-\frac{Q_2^2}{h_2^2} + r g' h_2\right) h_{2x} = v \frac{\partial}{\partial x}\left[h_2 \left(\frac{Q_2}{h_2}\right)_x\right], \tag{29}$$

or

$$G(h_1, h_2, Q_1, Q_2, r) h_{1x} = -\frac{v}{h_1}\left(\frac{Q_2^2}{h_2^3} - r\right)\frac{\partial}{\partial x}\left[h_1 \left(\frac{Q_1}{h_1}\right)_x\right] - \frac{r v}{h_2}\frac{\partial}{\partial x}\left[h_2 \left(\frac{Q_2}{h_2}\right)_x\right], \tag{30}$$

$$G(h_1, h_2, Q_1, Q_2, r) h_{1x} = -\frac{v}{h_2}\left(\frac{Q_1^2}{h_1^3} - 1\right)\frac{\partial}{\partial x}\left[h_2 \left(\frac{Q_2}{h_2}\right)_x\right] - \frac{r v}{h_1}\frac{\partial}{\partial x}\left[h_1 \left(\frac{Q_1}{h_1}\right)_x\right], \tag{31}$$

where

$$G(h_1, h_2, Q_1, Q_2, r) = \left(\frac{Q_1^2}{h_1^3} - g'\right)\left(\frac{Q_2^2}{h_2^3} - r g'\right) - r^2, \tag{32}$$

and $g' = g(\rho_1 - \rho_3)/\rho_1$ is the reduced gravity. Noticing that $F_1^2 = Q_1^2/g' h_1^3$ and $F_2^2 = Q_2^2/g' h_2^3$, $G = 0$ is the critical condition (16) for inviscid waves to be stationary in a two and a half layer system. It can be shown that $G > 0$ for BB flow or PP flow, and $G < 0$ for BP flow.

Scaling (28) and (29) with the following scales: h_{1a} for vertical length scale, $\sqrt{g' h_{1a}}$ for velocity scale, and $v/\sqrt{g' h_{1a}}$ for the horizontal length scale, the non-dimensional set of equations can be written as

$$\left(-\frac{Q_1^2}{h_1^2} + h_1\right) h_{1x} + r h_1 h_{2x} = \frac{\partial}{\partial \mathrm{x}}\left[h_1 \frac{Q_1}{h_1}\right)_x\Bigg], \tag{33}$$

$$r h_2 h_{1x} + \left(-\frac{Q_2^2}{h_2^2} + r h_2\right) h_{2x} = \frac{\partial}{\partial \mathrm{x}}\left[h_2 \left(\frac{Q_2}{h_2}\right)_x\right]. \tag{34}$$

The boundary conditions at the leading edge of a

shock are

$$h_1(\mathrm{x}=-\infty)=1; \qquad h_2(\mathrm{x}=-\infty)=h_{2\mathrm{a}}, \tag{35}$$

$$h_{1x}(x=-\infty)=0; \qquad h_{2x}(x=-\infty)=0, \tag{36}$$

where $h_{2\mathrm{a}}$ is the upper layer upstream depth scaled with $h_{1\mathrm{a}}$, the lower layer depth upstream of a shock. At the trailing edge of a shock, one expects that both interfaces become flat, i.e.,

$$h_{1x}(x=\infty)=0, \qquad h_{2x}(x=\infty)=0, \tag{37}$$

but the final depths $h_1(x=\infty)$ and $h_2(x=\infty)$ are unknown. A steady shock in a two and a half-layer flow is specified by the pair of second order non-linear ordinary differential equations (33, 34) and corresponding boundary conditions (35–37). The viscosity coefficient v does not appear in eqs. (33) and (34), which suggests that a two layer shock is pseudoinviscid in nature, i.e., that only the shock width is influenced by the magnitude of the viscosity.

The analytical solution for weak shocks and numerical solutions for shocks with finite amplitude will be discussed in the remaining parts of this section.

3.2. *Weak shock solutions*

For a weak shock, i.e., a shock with conjugate states near one of the branches of the critical curve, using $h_1=h_{1\mathrm{c}}+\eta$ and $h_2=h_{2\mathrm{c}}+\xi$, one can expand eqs. (33) and (34) about the critical depths $h_{1\mathrm{c}}$ and $h_{2\mathrm{c}}$, which are defined by

$$G(h_{1\mathrm{c}}, h_{2\mathrm{c}}, Q_1, Q_2, r)=0. \tag{38}$$

To the lowest order, we obtain

$$-3\left[\left(\frac{Q_2^2}{h_{2\mathrm{c}}^3}-r\right)\frac{Q_1^2\eta}{h_{1\mathrm{c}}^4}+\left(\frac{Q_1^2}{h_{1\mathrm{c}}^3}-1\right)\frac{Q_2^2\xi}{h_{2\mathrm{c}}^4}\right]\eta_x = \frac{Q_1}{h_{1\mathrm{c}}^2}\left(\frac{Q_2^2}{h_{2\mathrm{c}}^3}-r\right)\eta_{xx}+\frac{\mathrm{r}Q_2}{h_{2\mathrm{c}}^2}\xi_{xx}, \tag{39}$$

$$-3\left[\left(\frac{Q_2^2}{h_{2\mathrm{c}}^3}-r\right)\frac{Q_1^2\eta}{h_{1\mathrm{c}}^4}+\left(\frac{Q_1^2}{h_{1\mathrm{c}}^3}-1\right)\frac{Q_2^2\xi}{h_{2\mathrm{c}}^4}\right]\xi_x = \frac{rQ_1}{h_{1\mathrm{c}}^2}\eta_{xx}+\frac{Q_2}{h_{2\mathrm{c}}^2}\left(\frac{Q_1^2}{h_{1\mathrm{c}}^3}-1\right)\xi_{xx}. \tag{40}$$

Note that the above equations are coupled second order differential equations with some quadratic non-linear terms. A balance of linear and non-linear terms arises because our expansion involves two small parameters: shock amplitude and shock width (SS95).

In eqs. (39) and (40), the left-hand sides are quadratic terms and the right-hand sides are viscous terms with second order derivatives. Therefore, eqs. (39) and (40) represent a local balance between the non-linear steepening tendency and the viscous diffusion of momentum.

Assuming $\eta=\hat{\eta}\tanh(x/L)$, and $\xi=\hat{\xi}\tanh(x/L)$, where $-\hat{\eta}$ and $-\hat{\xi}$ are upstream values of the perturbation depth in the lower and upper layer, from eqs. (39–40), we obtain

$$3\left[\left(\frac{Q_2^2}{h_{2\mathrm{c}}^3}-r\right)\frac{Q_1^2\hat{\eta}}{h_{1\mathrm{c}}^4}+\left(\frac{Q_1^2}{h_{1\mathrm{c}}^3}-1\right)\frac{Q_2^2\hat{\xi}}{)h_{2\mathrm{c}}^4}\right]\hat{\eta} = \frac{2}{L}\left[\frac{Q_1}{h_{1\mathrm{c}}^2}\left(\frac{Q_2^2}{h_{2\mathrm{c}}^3}-r\right)\hat{\eta}+r\frac{Q_2}{h_{2\mathrm{c}}^2}\hat{\xi}\right], \tag{41}$$

$$3\left[\left(\frac{Q_2^2}{h_{2\mathrm{c}}^3}-r\right)\frac{Q_1^2\hat{\eta}}{h_{1\mathrm{c}}^4}+\left(\frac{Q_1^2}{h_{1\mathrm{c}}^3}-1\right)\frac{Q_2^2\hat{\xi}}{h_{2\mathrm{c}}^4}\right]\hat{\xi} = \frac{2}{L}\left[r\frac{Q_1}{h_{1\mathrm{c}}^2}\hat{\eta}+\frac{Q_2}{h_{2\mathrm{c}}^2}\left(\frac{Q_1^2}{h_{1\mathrm{c}}^3}-1\right)\hat{\xi}\right]. \tag{42}$$

From eqs. (41) and (42), one obtains formulae for the shock width

$$L=\frac{2}{3\hat{\eta}}\frac{Q_1/(Q_2^2/h_{2\mathrm{c}}^3-r)^2/h_{1\mathrm{c}}^2+r^2Q_2/h_{2\mathrm{c}}^2}{Q_1^2(Q_2^2/h_{2\mathrm{c}}^3-r)^2/h_{1\mathrm{c}}^4+rQ_2^2(Q_1^2/h_{1\mathrm{c}}^3-1)/h_{2\mathrm{c}}^4} \tag{43}$$

and the displacement ratio

$$\frac{\hat{\eta}}{\hat{\xi}}=\frac{Q_2^2/h_{2\mathrm{c}}^3-r}{r}. \tag{44}$$

Some important information can be learned from this weak shock solution. Using (44), and setting the denominator in eq. (43) equal to zero,

$$\frac{Q_2^2}{h_{2\mathrm{c}}^3}=r\left[1-\left(\frac{Q_2^2h_{1\mathrm{c}}^4}{Q_1^2h_{2\mathrm{c}}^4}\right)^{1/3}\right] \tag{45}$$

or

$$F_{2\mathrm{s}}^2=r\left[1-\left(\frac{F_{2\mathrm{s}}^2h_{1\mathrm{c}}}{F_{1\mathrm{s}}^2h_{2\mathrm{c}}}\right)^{1/3}\right], \tag{46}$$

where $(F_{1\mathrm{s}}, F_{2\mathrm{s}})$ is a special point on the internal branch of the critical curve. At this point $L=\infty$, so that a weak shock solution does not exist. Above this point ($F_2>F_{2\mathrm{s}}$ or $F_1<F_{1\mathrm{s}}$), the denominator in (43) is negative and to have a positive length scale, η must be negative (i.e., a drop of lower interface). Similarly, below this singular

point, we require $\eta > 0$ (i.e., a rise of lower interface). The significance of the singular point is clear in eqs. (41), (42). At the singular point, the second order non-linear terms become zero, which means non-linear steepening is absent. Therefore, no shock can form.

For an internal shock, $r > Q_2^2/h_{2c}^3 > 0$. Therefore, eq. (44) indicates that across an internal shock, the magnitude of the depth change in the lower layer is always smaller than that in the upper layer, and they are of opposite sign.

For an external shock, the depth changes have the same sign and the amplitude ratio (44) can be less than 1 or greater than 1, depending on its position on the diagram (Fig. 2). Along the lower-right part of the external branch, $Q_2^2/h_{2c}^3 - r < r$, the expansion of the lower layer dominates. Along the upper-left part of the external branch, $Q_2^2/h_{2c}^3 - r > r$, the expansion of the upper layer is more pronounced. In the middle part, $Q_2^2/h_{2c}^3 - r \sim r$, the expansions of the 2 layers are comparable.

In summary, the weak shock solution suggests that there are five types of two layer shocks: (a) internal jump, (b) internal drop, (c) external lower layer jump, (d) external two layer jump, and (e) external upper layer jump. The boundaries between weak type "c", "d", or "e" shocks are gradual. Notice that the weak shock solution is only valid near the critical curve. The regions with valid weak shock solutions and the 5 different types of weak shocks are schematically shown on Fig. 2.

If one tries to compute the Bernoulli change in each layer directly from the end state using the first order solutions, zero Bernoulli change will be obtained. This is not a surprise, because Bernoulli changes across a shock are higher order terms (SS95). Bernoulli losses across a two layer shock can be derived however from a 'process integration' based on the weak shock solution (43) and (44). Similar to the rigid lid case (Part I), to the lowest order, the Bernoulli losses can be expressed as

$$\Delta B_1 = \frac{Q_1}{h_{1c}^3} \int_a^b (\eta_x)^2 \, dx, \tag{47}$$

$$\Delta B_2 = \frac{Q_2}{h_{2c}^3} \int_a^b (\xi_x)^2 \, dx. \tag{48}$$

Using (44), (47), and (48),

$$\Delta B_1 = -\frac{3Q_1}{\hat{\eta} L} \left(\frac{\hat{\eta}}{h_{1c}} \right)^3, \tag{49}$$

$$\Delta B_2 = -\frac{3Q_2}{\hat{\xi} L} \left(\frac{\hat{\xi}}{h_{2c}} \right)^3. \tag{50}$$

As in the rigid lid case, eqs. (49) and (50) verify that Bernoulli changes in both layers are negative across a 2-layer shock.

Using (49) and (50), the ratio of Bernoulli changes in the lower and upper layer can be expressed as

$$\frac{\Delta B_1}{\Delta B_2} = \frac{Q_1}{Q_2} \left(\frac{\hat{\eta}}{\hat{\xi}} \right)^2 \left(\frac{h_{2c}}{h_{1c}} \right)^3. \tag{51}$$

Using (44), eq. (51) can be written in Froude numbers as

$$\frac{\Delta B_1}{\Delta B_2} = \sqrt{\frac{F_{1c}}{F_{2c}}} \left(\frac{F_{2c}^2 - r}{r} \right)^2 \left(\frac{h_{2c}}{h_{1c}} \right)^{1.5}, \tag{52}$$

where $F_{1c} = Q_1/h_1^{1.5}$ and $F_{2c} = Q_2/h_2^{1.5}$.

For an internal shock, $[(F_{2c}^2 - r)/r]^2 \sim 1$, so the Bernoulli change ratio is determined mostly by the Froude number ratio and the depth ratio. It will be shown that typically, for an internal jump,

$$\sqrt{\frac{F_{1c}}{F_{2c}}} \left(\frac{h_{2c}}{h_{1c}} \right)^{1.5} \gg 1$$

and for an internal drop,

$$\sqrt{\frac{F_{1c}}{F_{2c}}} \left(\frac{h_{2c}}{h_{1c}} \right)^{1.5} \ll 1,$$

so that the Bernoulli drop is strongly concentrated in the expanding layer.

For an external shock, the 3 factors in (52) can be equally important. As an example, for two layer flow with equal depth, if $F_{1c} = 1.5$ and $F_{2c} = 0.7817$, we have $\Delta B_1/\Delta B_2 = 0.07 \ll 1$, i.e., viscous dissipation in the upper layer is dominant; but if $F_{1c} = 1.05$ and $F_{2c} = 1.71$, we have $\Delta B_1/\Delta B_2 = 18.7 \gg 1$, i.e., viscous dissipation in the lower layer is much stronger.

3.3. *Tail modes in finite amplitude shocks*

In a finite amplitude shock, eqs. (28) and (29) are non-linear. However, at the two edges of a shock, assuming that the slopes of the interfaces

are very gentle, one can linearize these equations around the initial or final states. We define $h_1(x) = H_{10} + h_1'(x)$ and $h_2(x) = H_{20} + h_2'(x)$ with $h_1' \ll H_{10}$ and $h_2' \ll H_{20}$, where H_{10} and H_{20} are the upstream/downstream depths of the lower and upper layers.

The linearized equations can be written as

$$\left(-\frac{Q_1^2}{H_{10}^3} + 1 \right) h_{1x}' + r h_{2x}' = -\frac{Q_1}{H_{10}^2} h_{1xx}', \tag{53}$$

$$r h_{1x}' + \left(-\frac{Q_2^2}{H_{20}^3} + r \right) h_{2x}' = -\frac{Q_2}{H_{20}^2} h_{2xx}'. \tag{54}$$

Using $h_1'(x) = \hat{h}_1 e^{\lambda x}$ and $h_2'(x) = \hat{h}_2 e^{\lambda x}$ in eqs. (53) and (53), one can obtain the eigenvalues:

$$\lambda_{\text{int}} = \frac{b + \sqrt{b^2 - 4aG}}{2a}, \tag{55}$$

$$\lambda_{\text{ext}} = \frac{b - \sqrt{b^2 - 4aG}}{2a}, \tag{56}$$

where

$$a = Q_1 Q_2 / H_{10}^2 H_{20}^2, \tag{57}$$

$$b = \frac{Q_2}{H_{20}^2} \left(\frac{Q_1^2}{H_{10}^3} - 1 \right) + \frac{Q_1}{H_{10}^2} \left(\frac{Q_2^2}{H_{20}^3} - r \right), \tag{58}$$

$$G = \left(\frac{Q_1^2}{H_{10}^3} - 1 \right) \left(\frac{Q_2^2}{H_{20}^3} - r \right) - r^2. \tag{59}$$

For a given initial state, there are two λ's. Each λ corresponds to a viscous normal mode. We refer to λ_{ext} as the external tail mode eigenvalue, and λ_{int} as the internal tail mode eigenvalue.

The ratio of depth departures can be solved for a specified λ. Using (54),

$$\frac{\hat{h}_2}{\hat{h}_1} = \frac{Q_1^2}{H_{10}^3} - 1 - \frac{\lambda Q_1}{H_{10}^2}. \tag{60}$$

For a given mode, the sign of $\hat{h}_2/\hat{h}_1$, indicates the phase relations between 2 layers.

After algebraic manipulation, it can be shown that $b^2 - 4aG > 0$, i.e., λ is always real. The signs of the eigenvalues are listed in Table 1. Real λs indicate that the viscous tail modes are either growing or decaying. Taking the flow direction as the positive direction of the x coordinate, we have $x < 0$ towards the leading edge, and $x > 0$ towards the trailing edge.

At the leading edge, $x < 0$, a positive λ indicates that the flow depths converge to their upstream values as $x \to -\infty$, and a negative λ indicates that the flow depths diverge (Fig. 3). Therefore, at the leading edge of a shock, we refer to modes with $\lambda > 0$ as convergent tail modes, and modes with $\lambda < 0$ as divergent tail modes. Similarly, at the trailing edge, the tail modes with positive λs are divergent, and those with negative λs are convergent. We assume that only convergent modes are active modes at each edge. The coefficients of the divergent modes must be set to zero.

It is instructive to compare the viscous tail mode equations (53) and (54) with the inviscid linear wave eqs. (10), (11). They have a similar form except the time dependent terms in the linear wave equations are replaced by viscous terms. The linear wave equations indicate a balance among propagation, advection, and pressure gradient forces. Similarly, the viscous equations indicate a balance among viscous forces, advection, and pressure gradient forces. The importance of the viscous force in the balance is evident. Without a viscous force, propagating wave modes would be swept into the shock from upstream or downstream. No inviscid steady solutions are possible except for flow precisely at the critical state.

The dual role of G in defining criticality (16 or 32) and in controlling the decay of tail modes (32, 55 and 56) gives rise to the following rules: A two layer shock can neither start from the BB regime and nor end in the PP regime, as convergent tail modes are not available to meet the boundary

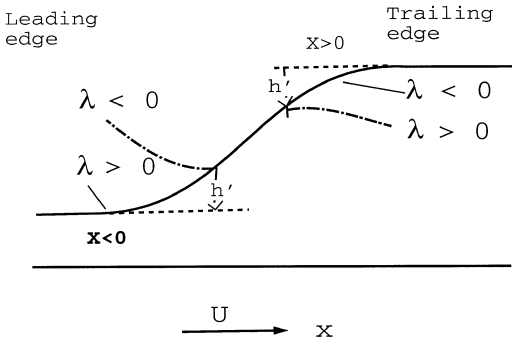

Fig. 3. Sketch of the tail modes. The arrow indicates the positive x direction and the flow direction. The solid curves are for decaying modes and the dot–dashed curves are for growing tail modes. At the leading edge $\lambda > 0$ is a decaying tail mode and $\lambda < 0$ is a growing tail mode, and at the trailing edge, $\lambda > 0$ is a growing mode and $\lambda < 0$ is a decaying mode.

condition at infinity. Based on the critical curves crossed by a shock trajectory, two layer shocks can be classified into three categories: Internal shocks, from BP to BB, cross the internal critical curve. They have one active tail mode at the leading edge and two active tail modes at the trailing edge. External shocks, from PP to BP, cross the external critical curve. They have 2 active tail modes at the leading edge and one active tail at the trailing edge. Two-mode shocks, from PP to BB, cross both critical curves. They have two active modes at both edges. It will be demonstrated later that although two-mode shocks are mathematical solutions of the viscous shock model, they are physically inaccessible.

Based on the nature of the tail modes, we can also conclude that it is impossible to have a monotonic shock from BP to BP, although there is a convergent tail mode at each end. At the leading edge, an internal tail mode is the convergent mode and at the trailing edge, an external tail mode is a convergent mode. However, an internal tail mode has an opposite phase relation between the two interface perturbations while an external tail mode has an in-phase relation. To match both tail modes then, one of the interfaces would have to change slope in the middle of the shock. Thus, the matching between an internal tail mode and an external tail mode is impossible in a monotonic shock.

These shock "rules" prohibit six of the nine possible transitions between the three states of criticality (BB, BP and PP). Only 2 types of transition remain; the internal and external shock. The former crosses the internal critical curve while the latter crosses the external critical curve. The 2-mode shock is impossible for other reasons.

The terms "internal shock" or "external shock" do not relate simply to the internal or external linear waves or tail modes. As indicated by the tail modes at the two ends, none of these shocks are purely "internal" or "external" in a linear sense, because both types of tail modes are involved in each type of shock.

4. Shock regime diagram

Using the rules developed above, we can attempt to classify two layer shocks on a shock regime diagram. A shock regime diagram for two layer flow under a rigid lid was discussed by Mehrotra (1973), and such a diagram was created in Part I based first on a wave steepening condition and then refined with a viscous model (JS00b). The steepening condition in Part I was the requirement that a shock start with supercritical conditions and have a range of mass-conserving total-depth-conserving subcritical end-states available.

In two-layer flow with a passive third layer, things are more complex. TM conservation plays the rôle of total-depth conservation and the tail-mode "rules" play the role of the super- to subcritical condition. These 2 conditions together comprise a "steepening condition". The TM conservation tells us which end states may be possible from a specified pre-shock state and the tail-mode "rules" tell us whether these end states allow shock solutions with convergent tail modes to be constructed.

As with the rigid lid case, we must remember that the steepening condition is a necessary but not sufficient condition for shock existence. We shall see that the steepening condition is not as useful here as it was in Part I as it is too "generous". For example, it predicts the existence of internal shocks from large portions of BP, whereas only a small portion of BP actually allows such shocks. Because of the weakness of the steepening constraint, we will put more emphasis on using the full viscous equations to determine shock existence. A shock-allowable state defined in this context is a state for which a steady shock solution can be obtained based on the viscous model.

The shock diagram for a two and a half layer flow is shown on Fig. 4 (notations are listed in Table 1). The critical curves divide this diagram into a BB regime, BP regime, and PP regime. According to the "rules", flow in the BB regime is not allowed to have shocks. Thus, we require no further investigation of this region. The subdivision of the BP and PP regimes, numerical strategies, and shock features will be addressed in the subsequent parts of this section.

4.1. Subdividing the BP regime

2 methods can be used to subdivide the BP regime: the TM constraint on steepening and numerical calculation. According to viscous tail mode theory, if the pre-shock flow is in the BP

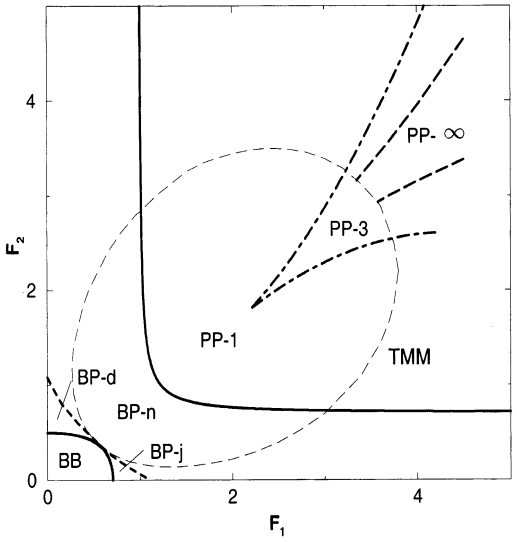

Fig. 4. Froude number regime diagram for two-layer shocks. The internal and external branches of the critical curve (in bold-solid) divide the diagram into BB, BP, and PP regimes. The marginal curve (in bold-dashed) for $K = 1$ and $r = 0.5$ divides the BP regime into three subregimes: BP-j regime, BP-d regime, and BP-n regime; The PP regime is divided into three sub-regimes: PP-1, PP-3, and PP-∞. The closed curve (dashed) is the TMM curve (for $K = 1$), outside of which the TM curve of each point has a BB portion.

regime, the post-shock flow must be in the BB regime. A dashed closed curve (TMM) is shown on the regime diagram (Fig. 4). This is a marginal curve representing flow states with their TM curve tangential with the internal critical curve (at the point F_{10}, F_{20}). For simplicity, we refer to it as the TMM curve. TM curves cannot cross the TMM curve. The portion of BP inside the TMM curve cannot have a BB conjugate state, which means that a shock is impossible. If one draws a TM curve from a flow state lying in BP outside the TMM curve, there must be a portion of the TM curve lying in the BB regime. This is a necessary condition for shock existence. The actual existence of shocks starting in this subregime must be determined using numerical integration.

4.1.1. Numerical integration. In order to apply boundary conditions (35–37) to the numerical integration, a method is needed to bring the boundary points from infinity to some finite distance. One approach is to use the normal mode theory discussed in the last section. With the upstream flow in the BP regime, only the internal viscous tail mode is convergent at the leading edge. Therefore, near the leading edge, we have

$$h_1(x) = 1 + \hat{h}_1 e^{\lambda_{\text{int}} x}, \tag{61}$$

$$h_2(x) = h_{2a} + \hat{h}_2 e^{\lambda_{\text{int}} x}, \tag{62}$$

where λ_{int} can be solved from eq. (55), and the relation between $\hat{h}_1$ and $\hat{h}_2$ can be solved from eq. (60).

Instead of integrating from $x = -\infty$, we start the integration from $x = 0$. Using (61) and (62), we obtain the boundary conditions at $x = 0$:

$$\begin{aligned} &h_1 = 1 + \hat{h}_1, \qquad h_2 = h_{2a} + \hat{h}_2, \\ &h_{1x} = \lambda_{\text{int}} \hat{h}_1, \qquad h_{2x} = \lambda_{\text{int}} \hat{h}_2. \end{aligned} \tag{63}$$

The only free parameter in the above equations is $\hat{h}_1$, which can be arbitrarily specified, as long as it is small enough to satisfy the linear assumptions (e.g., ± 0.001 has been used in this study). Based on these boundary conditions, eqs. (33–34) can be integrated using finite difference methods. The integration continues until a new equilibrium state is nearly reached. The end point must satisfy the following criteria:

$$\begin{aligned} &h_{1x}(x = x_b) = h_{2x}(x = x_b) = O(\varepsilon), \\ &|TM_a - TM_b| = O(\varepsilon), \end{aligned} \tag{64}$$

where ε is a small number. A upstream state is classified as unacceptable if the solution diverges downstream.

Based on the numerical solutions for a given pre-shock depth ratio $K = 1/h_{2b}$, a marginal curve can be derived which is tangential to the internal branch of the critical curve at the point (F_{1s}, F_{2s}). This singular point is given by weak shock theory (46). Flow in the BP regime can be divided into three sub-regimes by this marginal curve, namely, BP-j regime, BP-d regime, and BP-n regime. As for the rigid lid case (Jiang and Smith, 2001), for a given depth ratio, this marginal curve represents a shock bifurcation. For any point on the curve, its conjugate state lies on the far side of the internal critical curve. This marginal curve shows strong dependence on the depth ratio K. The marginal curve for $K = 1$ is shown in Fig. 4.

4.1.2. BP-j: the jump regime. In the BP-j regime, flow in the lower layer is more active, i.e., either faster, or thinner, or both. An internal jump occurs

with a rise of the lower interface and a slight drop of the upper interface. An example is shown in Fig. 5. The "TM" value is decreased in the first half of the shock due to the upstream pointing total viscous force, and recovers its initial value by the end of the shock due to the reversal of the internal viscous force in the trailing half of the shock. The Bernoulli variations in two layers are initially of opposite sign similar to the the variation of "TM". The final Bernoulli changes across the shock in both layers are negative with the Bernoulli loss in the lower layer dominant. The variation of viscous forces in the two layers is consistent with the variations of TM and Bernoulli changes.

4.1.3. BP-d: the drop regime. The internal drop regime is characterized by $F_1 < F_2$, i.e., a more active upper layer. An internal shock occurs with a drop of the lower interface and a slight rise of the upper free surface. An example is shown in Fig. 6. The Bernoulli loss in the upper layer is much larger than in the lower layer. The post-shock flow is in the BB regime.

Solutions for the internal jump and drop are qualitatively similar to the weak shock solutions described in the last section. While some previous shock theories predicted multiple conjugate states for internal shocks (e.g., YG55), the uniqueness of an internal shock is clear from the point of view of the viscous shock theory. There is only one convergent tail mode at the leading edge, which makes the boundary condition (at $x = 0$) unique. Thus, the shock is unique.

4.1.4. BP-n: the no-shock regime. As for the rigid lid case (Mehrotra, 1973; Jiang and Smith, 2001), a large portion of the BP regime is found to not allow shocks. In this BP-n subregime, a finite amplitude perturbation riding on the basic flow is unable to steepen and form a steady shock. For pre-shock states inside TMM, TM trajectories cannot even enter BB. For the other pre-shock states in BP-n, trajectories enter BB but pass out

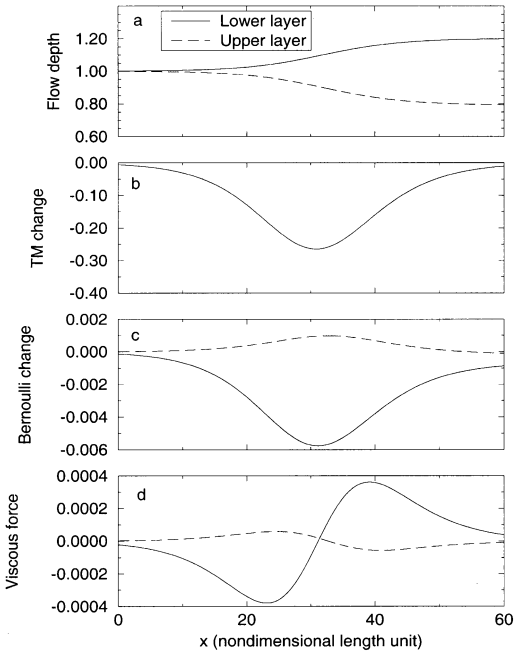

Fig. 5. An internal jump solution with $F_1 = 0.8$, $F_2 = 0.1$, $K = 1$, $r = 0.5$; (a) flow depths; (b) % of total momentum (TM) change, i.e., $100 \times (\mathrm{TM} - \mathrm{TM_a})/\mathrm{TM_a}$; (c) % of Bernoulli changes, i.e., $100 \times (B_1 - B_{1a})/B_{1a}$ and $100 \times (B_2 - B_{2a})/B_{2a}$; (d) viscous forces. The values for the upper layer are dashed.

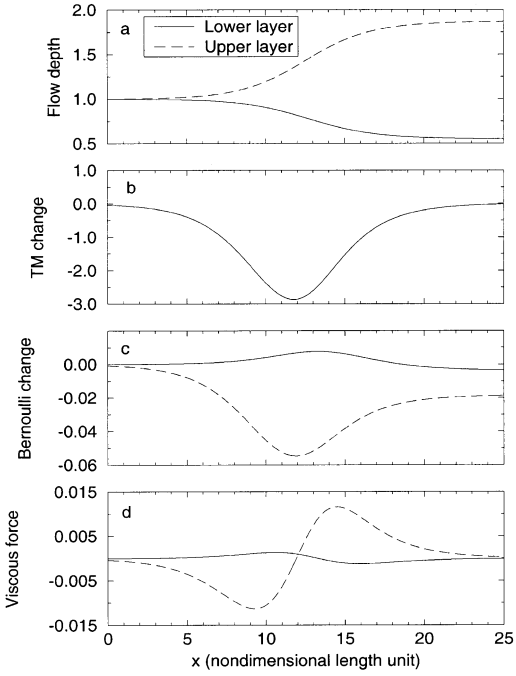

Fig. 6. An internal drop solution. The same quantities are plotted as in Fig. 5 except $F_2 = 0.8$, $F_1 = 0.1$, $K = 1$, $r = 0.5$.

the other side into BP again before reaching an end state. In either case, no shock exists.

4.2. Subdividing the PP regime

4.2.1. Reverse integration. The strategy for subdividing the regime diagram becomes more complicated for regime PP. With two convergent tail modes at the leading edge, a proper combination of the two modes has to be found, i.e.,

$$h_1(x) = 1 + \hat{h}_1(e^{\lambda_{int}x} + \beta e^{\lambda_{ext}x}), \tag{65}$$

$$h_2(x) = h_{2a} + \hat{h}_1(\gamma_1 e^{\lambda_{int}x} + \gamma_2 \beta e^{\lambda_{ext}x}), \tag{66}$$

where β is a unknown coefficient. The coefficients γ_1 and γ_2 are ratios between the departures from the upstream depths for internal and external modes, respectively, and can be derived from linear eqs. (53) and (54).

One can obtain a set of boundary conditions at $x = 0$:

$$\begin{aligned} h_1 &= 1 + \hat{h}_1(1 + \beta), \\ h_2 &= h_{2a} + \hat{h}_1(\gamma_1 + \gamma_2 \beta), \\ h_{1x} &= \hat{h}_1(\lambda_{int} + \beta \lambda_{ext}), \\ h_{2x} &= \hat{h}_1(\gamma_1 \lambda_{int} + \beta \gamma_2 \lambda_{ext}). \end{aligned} \tag{67}$$

Notice that β is the only free parameter to be determined. One straightforward approach is the so called shooting method: try every possible β, until the right one is found, that is, until a final equilibrium state can be reached. The primary assumption of the shooting method is that solutions are well behaved, which means that corrections to β can be made based on previous end-state estimations. Unfortunately, due to the highly non-linear nature of the governing eqs. (33–34) and the special end-state boundary condition (at infinity), it is often found that a fairly accurate estimate of β is required for a successful convergent iteration.

Fortunately, there is a better way to find the conjugate states and verify their uniqueness. For a given point in PP with a specified depth ratio, its TM conservation curve is a closed curve which spans BP and PP (Fig. 7). Any point on the PP portion of the curve must have its conjugate state(s) on the BP portion of the curve. Therefore, instead of starting the integration from the PP portion, one can start from the BP portion and do the integration in reverse. The equilibrium state for this type of integration will be a point along the PP portion of the TM curve. The advantage of reverse integration is that the downstream convergent tail mode of BP flow is unique. For a given pre-shock state "A", the integration gives a point along the PP portion of the TM curve. We define the distance of the end-state equilibrium point from "A" as D_A, positive clockwise and negative counterclockwise. The conjugate state(s) of "A" will be those points in BP having $D_A = 0$ as equilibrium states. On Fig. 7, point C is a interception of the critical curve and TM curve, we define the distance of a point on the BP portion of TM curve from C as D_C. For point A and point B, the results of this reverse integration are plotted on Fig. 8. Obviously, for point A, the curve passes over zero once, which indicates that point A has a unique conjugate state and for point B, the curve passes over zero three times, which suggests that point B has three conjugate states. Based on the numbers of conjugate states, flow in the PP regime can be divided into three sub-regimes: PP-1 (unique conjugate state), PP-3 (three conjugate states), and PP-∞ (infinity of conjugate states).

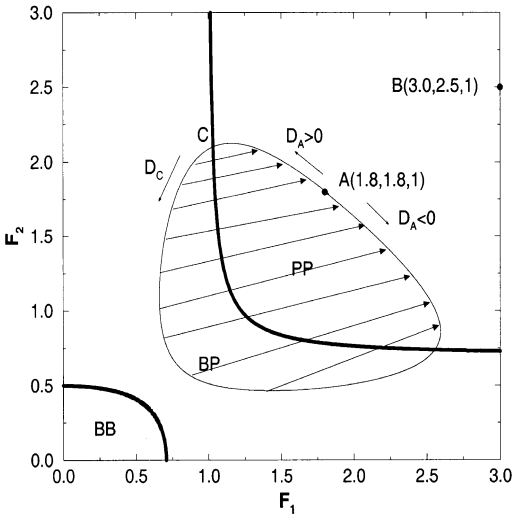

Fig. 7. Definition sketch for the reverse integration method. D_A is the distance from point A and positive along clockwise direction. D_c is the distance from point C along the TM curve. Arrows point from post-shock states to pre-shock states.

4.2.2. The PP-1 regime; unique conjugate states. As shown in Fig. 4, the PP-1 regime covers most of PP. Flow in this regime has a unique conjugate

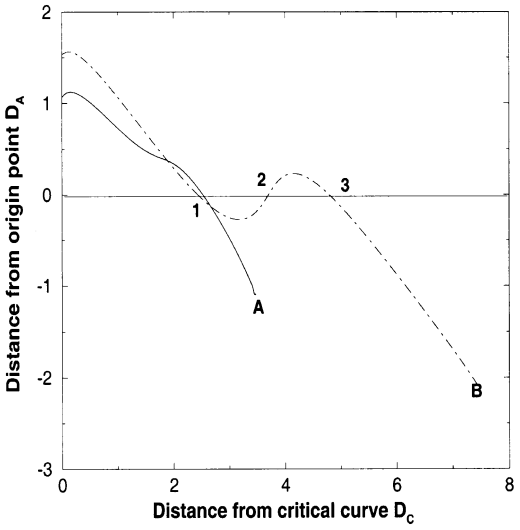

Fig. 8. Examples of reverse integration. Case A: $F_1 = 1.8$, $F_2 = 1.8$, $K = 1$; Case B: $F_1 = 3.0$, $F_2 = 2.5$, $K = 1$.

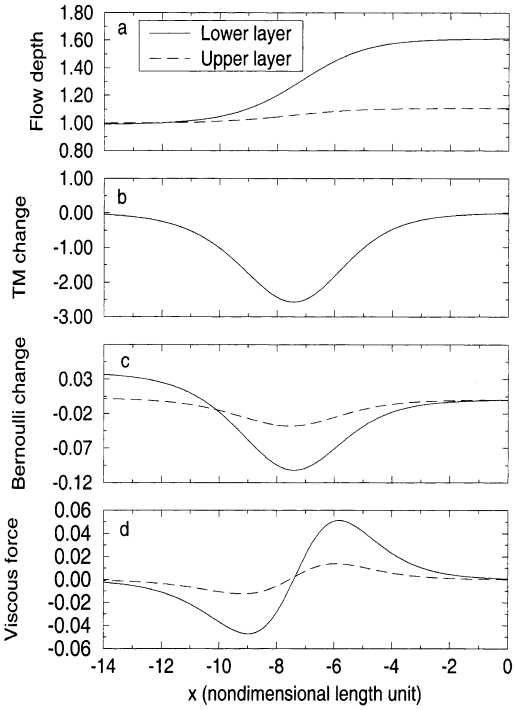

Fig. 9. Solution for an external type c shock. The same quantities are plotted as in Fig. 5 except $F_1 = 1.5$, $F_2 = 2$, $K = 1$, $r = 0.5$.

state in BP. Solutions in PP-1 are qualitatively similar to weak external shock solutions. Therefore, three types of shocks can be expected. For those flows with $F_1 \gg F_2$, there will be an external upper layer shock, which makes the flow even more asymmetric. With the lower interface almost unchanged, this type of shock is somewhat similar to a single layer shock above a passive lower layer. For those flows with $F_1 \ll F_2$, the shock will be an external lower layer type, which makes F_1 even smaller. In this type of shocks, the upper layer is almost passive: changing its mean elevation but only slightly its thickness. For flows with $F_1 \sim F_2$, there will be an external two layer shock with comparable expansions of two layers.

Examples for these three types of shocks are shown in Figs. 9–11. Notice that the x coordinate is negative due to the reverse integration. As the upstream flow is changed from backward shear to forward shear, the shock changes from type "c", to type "d", and finally to type "e".

4.2.3. The PP-3 regime; three conjugate states. In the small V-shaped regime (Fig. 4), a catastrophe or cusp (Gilmore, 1981) is identified. In this regime, for each specified flow state, there are three conjugate states corresponding to type "c", type "d", and type "e" shock, respectively. Each point on the boundaries of the cusp corresponds to one isolated conjugate state and a doubly degenerate conjugate state. At the tip of the cusp, it has a triply degenerate conjugate state. For $K = 1$ and $r = 0.5$, the location of the tip is $(F_1, F_2) = (2.22 \pm 0.01, 1.82 \pm 0.01)$. This location varies with both K and r. For example, the location of the tip moves to $(F_1, F_2) = (2.54 \pm 0.01,\ 1.54 \pm 0.01)$ for $K = 0.5$, and moves to $(F_1, F_2) = (1.87 \pm 0.01, 2.04 \pm 0.01)$ for $K = 2$. To understand the structure of the cusp and physical features of conjugate states, a set of solutions has been computed for pre-jump points on a circle centered at $(F_1 = 0, F_2 = 0)$ and a radius of $\sqrt{F_1^2 + F_2^2} = 4$, which cuts through the PP-3 regime. Three types of solutions are illustrated in Fig. 12. One natural question is how to access the middle branch of solutions. In Section 5, we will show that if one slowly approaches the cusp from either side, the conjugate state will stick to either the lower layer jump or upper layer jump solution. Therefore, the only possible way to access the type "d" shock is by

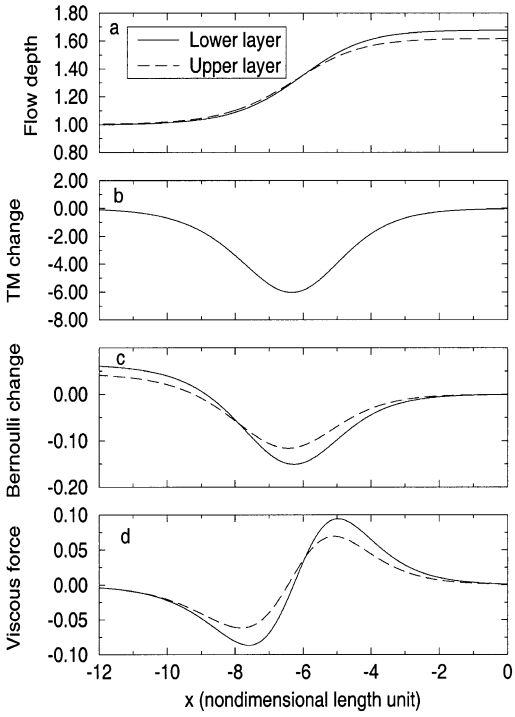

Fig. 10. Solution for an external type d shock. The same quantities are plotted as in Fig. 5 except $F_1 = 1.8$, $F_2 = 1.5$, $K = 1$, $r = 0.5$.

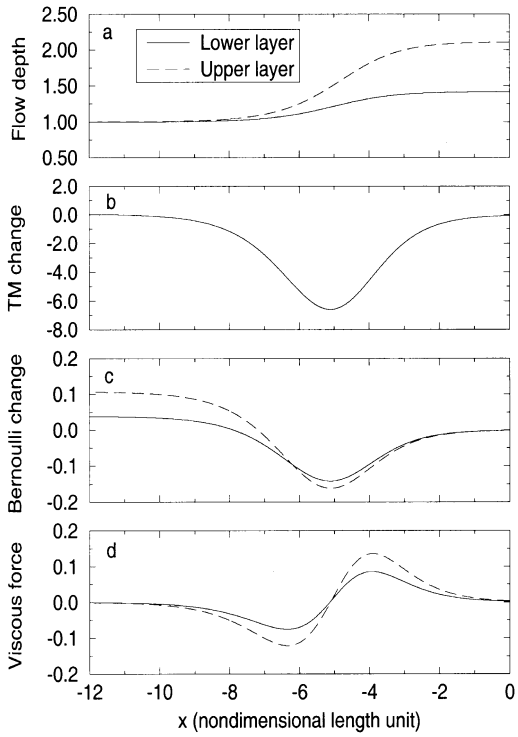

Fig. 11. Solution for an external type e shock. The same quantities are plotted as in Fig. 5 except $F_1 = 2.0$, $F_2 = 1.5$, $K = 1$, $r = 0.5$.

entering the cusp precisely through the peak of the cusp region, which is practically impossible.

4.2.4. The PP-∞ regime; an infinity of conjugate states. The viscous calculation shows that in a subregion external to the TMM curve, but within PP-3, type "d" shocks exist with end states in BB. As these shocks cross two critical curves, we call them two-mode shocks. Each pre-shock state in this subregion has an infinite number of end-states. We thus call this subregion, PP-∞. The mathematical reason for the infinity of end states is that all four tail modes are convergent (Subsection 3.3); giving one extra adjustable amplitude coefficient to satisfy the boundary conditions. All but one of these shocks is non-monotonic however.

This curious subregion lies on the "d" branch of PP-3, and is therefore inaccessible. For this reason, we have not carried out more detailed investigations of this subregion. We expect that real pre-shock states in PP-∞ will give rise to type "c" or "e" shocks with end states in BP.

5. Model comparisons

5.1. Comparison with shallow water simulations

5.1.1. Two and a half layer shallow water model. To further understand two layer shock dynamics and explore the proper way to simulate non-linear hydraulic phenomena, we compare steady 1-D viscous shock solutions with shock simulations in a time dependent 2-D shallow water model (SWM). We particularly focus on bow shocks in front of isolated hills. As is well known, as super-critical flow approaches a 2-D obstacle of finite height, a bow shock may appear in front of the obstacle (Baines, 1995; Jiang and Smith, 2000a). Although the simulation of 2-D flow requires more computing resources than 1-D flow, it allows the lateral dispersion of perturbations and a steady

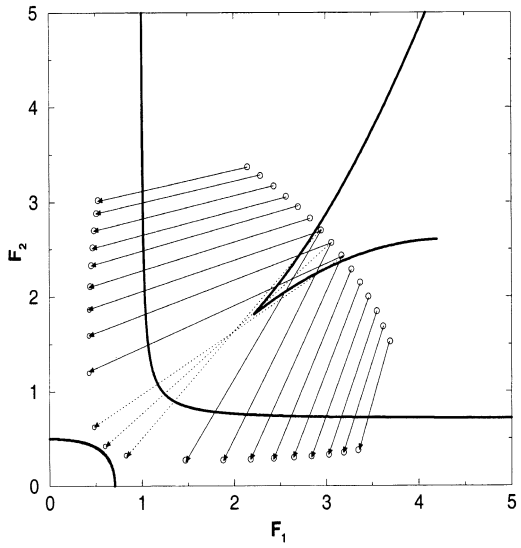

Fig. 12. A set of shock solutions for pre-shock conditions arrayed across the cusp. Three types of solutions are apparent, i.e., type c, type d, and type e. Points in the cusp have three conjugate states corresponding to three types of shocks.

state can be reached with stationary shocks located near the obstacle. Along the centerline, a bow shock is a normal shock, with pre-shock conditions approximately the same as the specified inflow conditions. The shock thickness is much less than the radius of curvature so the bow shock can be considered 1-D.

Two-layer flow with a free surface has been investigated in one dimension by Houghton and Isaacson (1968). They explicitly used YG's shock condition in their numerical formulation. With only one horizontal dimension in their study, no stationary shock was found upstream of the ridge.

The shallow water model used for this study has been described in Part I. A set of time dependent shallow water eqs. (4–6) are integrated in flux form. A flux-corrected transport (FCT) technique has been used to ensure that momentum and mass are conserved simultaneously. Further details can be found in SS93 and Schär and Smolarkiewicz (1996).

In this study, we use a bell shaped obstacle, specified by

$$h(x, y) = M/(1 + x^2 + y^2)^{3/2}, \tag{68}$$

where the $M = h_m/h_0$ is the nondimensional maximum height, (x, y) is horizontal dimensions scaled by the half width of the obstacle. The domain size is 80×40 with a spatial resolution of $DX = DX = 0.1$. Temporal resolutions, ranging from 0.005 to 0.025, are chosen to satisfy the numerical stability criterion. A typical run to a steady state lasts 40 nondimensional time units.

In order to obtain steady state solutions, we start the flow from rest, and integrate with 'zero gradient' boundary conditions along at the edges of the domain. The integration is carried out until a steady state is reached. The sensitivity of the steady state solutions to different boundary conditions has been tested, verifying that for such a large domain. the shock structures and other interior patterns are not influenced by the boundary conditions.

The control parameters for our simulations are: two Froude numbers F_1 and F_2, the nondimensional mountain height M, the flow depth ratio K $(=h_1/h_2)$, and the density step ratio r.

5.1.2. Steady state solutions. A few examples of bow shocks are shown in Fig. 13. For different cases, different Froude numbers and mountain height M have been chosen to generate the desired bow shocks. The upstream depth ratio and density step ratio were kept constant for all cases.

Case "a" shows that as an upstream flow in the BP-j regime approaches the hill, a steady bow shock appears, taking the form of an internal jump. The lower interface rises and the upper interface drops slightly. Case "b" shows a bow shock in the form of an internal drop with a drop of the lower interface and a rise of the upper interface. The upstream flow is in the BP-d regime.

Case "c" shows an external lower layer bow shock. The upstream flow is in the PP-1 regime and forward shear promotes the expansion of the lower layer $\delta h_1 = 1.2$, while the upper layer depth is almost unchanged $\delta h_2 < 0.05$. Case "d" shows an external two layer jump. The upstream flow is in the PP-1 regime and the two layers are equally active. The expansion of two layers are comparable ($\delta h_1 = 0.75$ and $\delta h_2 = 0.65$). Case "e" shows that with backward shear, an external upper layer jump forms in front of the obstacle. Most of the expansion occurs in the upper layer ($\delta h_1 = 0.3$ and $\delta h_2 = 1.5$).

Fig. 13 "f" and "g" show two runs with upstream flow in the cusp region. The upstream

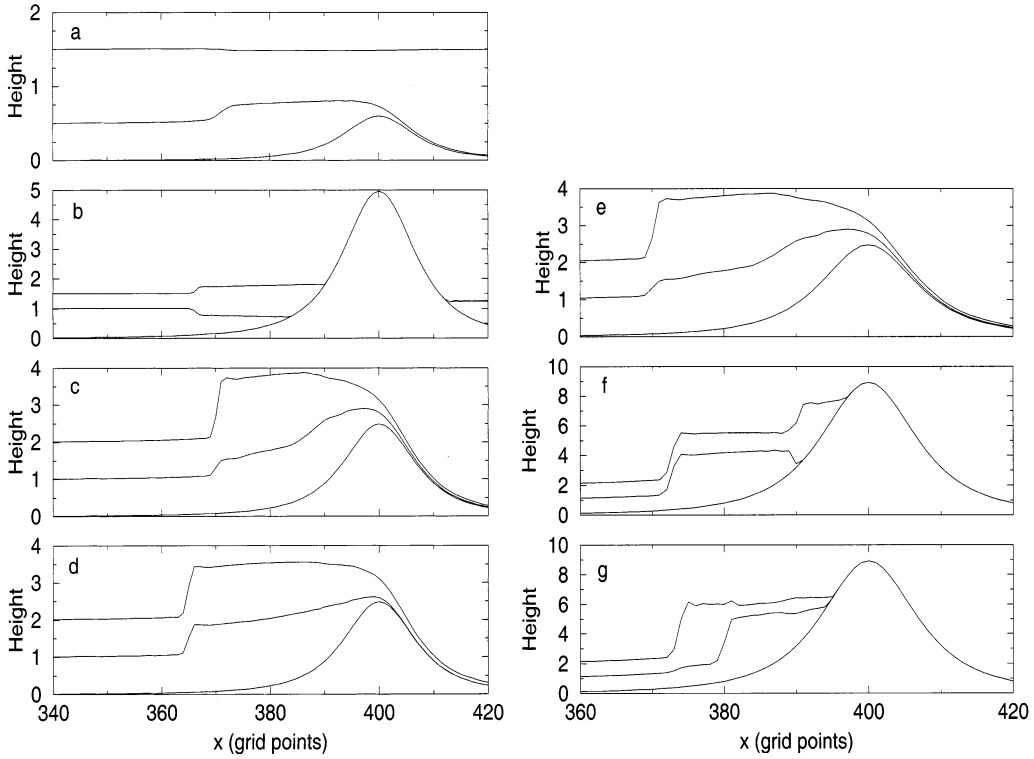

Fig. 13. Shallow water simulations along the center streamline. The obstacle and the lower and upper interfaces are shown as solid curves. Flow is from left to right. Only part of the upstream domain is shown. For all the cases, $K = 1$ and $r = 0.5$. (a) Internal jump: $F_1 = 0.8$ and $F_2 = 0.1$; (b) Internal drop: $F_1 = 0.1$ and $F_2 = 0.8$; (c) External lower-layer jump: $F_1 = 2.0$ and $F_2 = 2.0$; (d) External two-layer jump: $F_1 = 1.8$ and $F_2 = 1.5$; (e) External upper-layer jump: $F_1 = 2.0$ and $F_2 = 1.5$; (f) Jump-drop pair: $F_1 = 4 \cos 37.5^\circ$ and $F_2 = 4 \sin 37.5^\circ$; (g) Jump-jump pair: $F_1 = 4 \cos 40^\circ$ and $F_2 = 4 \sin 40^\circ$.

state of case "f" is of roughly equal distance from the two cusp boundaries. A lower layer jump occurs first with a transition from PP-3 to BP-n. The strong dissipation in the lower layer puts the post-shock flow close to the BP-d regime. After a short distance of adjustment, a second shock occurs which brings the flow into the BB regime. With flow in the upper layer more active, the second shock is an internal drop.

The upstream flow of case "g" is close to the lower boundary of the cusp. An upper layer jump occurs first with the lower layer almost unchanged. The post-jump flow is in the BP-n regime and close to the BP-j regime. An internal jump occurs after a short distance of adjustment.

5.1.3. Cusp and hysteresis. To investigate flow behavior around the cusp region, two special runs were performed with a slowly changing upstream flow. By changing the upstream boundary condition, we allow the ambient flow to slowly change along a circle in Fig. 14, with the origin at (0, 0) and a radius $\sqrt{F_1^2 + F_2^2} = 4$. In the first case, the pre-shock state is modified to move counter-clockwise. It begins at point A, reaches the cusp boundary at point D, the cusp center at C, the far cusp boundary at E and finally ends at B. In the second case, the pre-shock state begins at B and moves clockwise to A.

The rate of change can be measured by a time scale defined as $T = U/(\mathrm{d}U/\mathrm{d}t)$. Some other time scales can be constructed from control parameters are $T_1 = L/U$, $T_2 = a/U$, $T_3 = L/(U - C)$, where L is the domain length, a is the half width of the obstacle, and C is the external wave speed. In our simulation, $T = 600$, $T_1 < 40$, $T_2 < 5$, $T_3 < 80$.

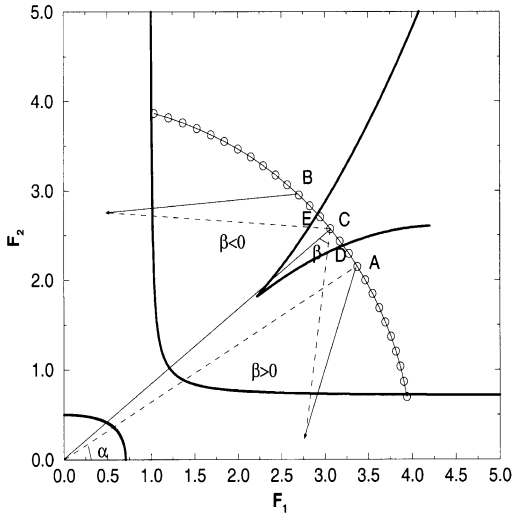

Fig. 14. A sequence of strong external shocks with pre-shock states lying on a circle with its origin at (0, 0) and a radius of $\sqrt{F_1^2 + F_2^2} = 4$. This circle intercepts the cusp boundary at point D and E. Angle α defines a radial to the pre-shock state. Angle β is the angle between the line passing from point C and origin (0, 0), and the line passing through the post-shock state and point C. Angle β is positive in counterclockwise direction.

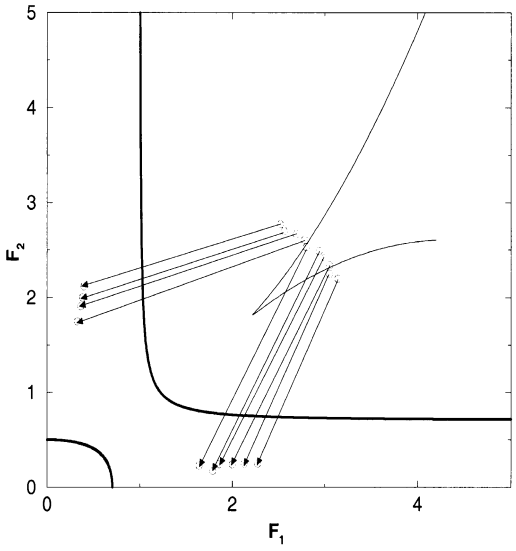

Fig. 15. A sequence of strong external bow shocks formed in the shallow water model as the shear in the upstream flow is slowly varied from reverse to forward. On the figure, the pre-shock state moves in a counter-clockwise fashion. The arrows point from pre-shock states to post-shock states. Note the abrupt change in post-shock state as the pre-shock state crosses the cusp boundary. Reference curves are as in Fig. 4.

Therefore, we believe that the change is slow enough to allow the flow to evolve through a sequence of near steady states.

The results are shown in Figs. 15, 16. Fig. 15 shows a run with flow speed changing along the circle in counterclockwise direction (i.e., from forward shear to backward shear). The arrows point from the pre-shock to post-shock state. Note that due to the slight slope of the underlying topography, the pre-shock flow states are slightly different than the specified upstream flow states, which are precisely on the circle. Initially, the shock is type "e", and it remains type "e" while the ambient flow goes into the cusp. Upon crossing the second boundary of the cusp, a sudden change occurs with the bow shock switching from type "e" to type "c".

To describe to the hysteresis, we define two angles α and β (Fig. 14). For both clockwise and counterclockwise runs, the results are plotted in Fig. 16. The solid curve represents viscous model predictions for initial states along the circle.

The viscous shock theory predicts a 3-branch solution. For the clockwise run (α decrease), the

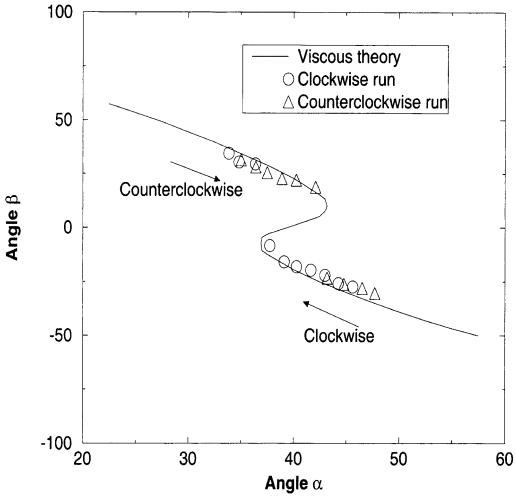

Fig. 16. Viscous shock solutions (in solid), clockwise SWM run (circles), and counterclockwise run (triangles). For the clockwise run, α decreases and β increases. For the counterclockwise run, α increases and β decreases.

bow shock evolves along the lower branch, and jumps to the upper branch after point E, which is the end of the lower branch solution. For the counterclockwise run (α increases), the bow shock remains on the upper branch until point D and then jumps to the lower branch. In both cases, the middle branch was never accessed.

These simulations agree with viscous shock theory predictions concerning the existence and position of the PP-3 regime. They also confirm our suspicion concerning the inaccessibility of type "d" solutions and the existence of hysteresis in the cusp region.

The good quantitative agreement between 1-D steady viscous shock theory and the 2-D time-dependent shallow water model (SWM) comes as a surprise. Unlike the viscous model, the SWM has no explicit viscosity and this allows shocks to steepen into jagged structures spanning only a few grid points. Numerical dissipation and diffusion must dominate in SWM shocks, constrained only by its flux-formulation (Schär and Smolarkiewicz, 1996). This agreement builds confidence that our results are robust, i.e., not overly sensitive to model formulation.

5.2. *Comparison with YG theory*

As discussed in Section 1, classical shock theories close the two layer shock problem by either assuming a certain momentum exchange formula or energy conservation in one layer. We compare our results with the former scheme by looking at YG's shock condition (YG55). YG assumed a special form of M_{12}, i.e.,

$$M_{12} = \tfrac{1}{2}\rho_2 g'(h_1' - h_1)(h_2' + h_2). \tag{69}$$

Substituting (69) into eqs. (23–24), we obtain the classical shock condition for a two and a half layer Boussinesq flow,

$$2F_1^2\frac{h_1' - h_1}{h_1} = \left(1 + \frac{h_1' - h_1}{h_1}\right)\left(2 + \frac{h_1' - h_1}{h_1}\right) \times \left(\frac{h_1' - h_1}{h_1} + r\frac{h_2' - h_2}{h_2}\Big/ K\right), \tag{70}$$

$$2F_2^2\frac{h_2' - h_2}{h_2} = r\left(1 + \frac{h_2' - h_2}{h_2}\right)\left(2 + \frac{h_2' - h_2}{h_2}\right) \times \left(K\frac{h_1' - h_1}{h_1} + \frac{h_2' - h_2}{h_2}\right), \tag{71}$$

where $K = h_1/h_2$ is the pre-shock layer depth ratio. An measure of the energy budget in a steady flow is the Bernoulli function along the interfaces. For a two and a half layer flow, the nondimensional (scaled with $g'h_0$) Bernoulli functions are defined as

$$B_1 = \tfrac{1}{2}U_1^2 + h_1 + rh_2, \tag{72}$$

$$B_2 = \tfrac{1}{2}U_2^2 + rh_1 + rh_2. \tag{73}$$

Using (70–73), one can obtain

$$\delta B_1 = -\frac{h_1F_1^2\varepsilon_1^3}{2(\varepsilon_1+1)^2(\varepsilon_1+2)}, \tag{74}$$

$$\delta B_2 = -\frac{h_2F_2^2\varepsilon_2^3}{2r(\varepsilon_2+1)^2(\varepsilon_2+2)}, \tag{75}$$

where δB_1 and δB_2 are Bernoulli changes in the lower layer, upper layer respectively, and $\varepsilon_1 = (h_1' - h_1)/h_1$ and $\varepsilon_2 = (h_2' - h_2)/h_2$ are proportional depth changes.

It can be demonstrated from YG's theory that for an internal jump, $\varepsilon_1 > 0$ and $\varepsilon_2 < 0$ and for an internal drop, $\varepsilon_1 < 0$ and $\varepsilon_2 > 0$. Therefore, from eqs. (74–75), there is an energy gain in the upper (lower) layer after an internal jump (drop) for a two and a half layer flow. Apparently the assumed momentum exchange formula (69) in YG's theory is problematic.

To compare YG and viscous theory, we revisit five of the examples shown in the last section. YG's predictions and the viscous shock theory predictions are listed in Table 2. The YG post-shock state were obtained by numerically solving eqs. (70) and (71). Also listed in Table 2 is M_{12}, the momentum exchange computed from viscous shock theory (25) and scaled with $g'(h_1' - h_1)(h_2 + h_2')$, which is the YG's assumption of interfacial momentum exchange.

For flow in the BP-j (case (a) regime and BP-d (case (b) regime, YG theory predicts three end states. Only two of them are shown in the table. The third one represents an internal two-layer jump with Bernoulli gain in both layers, which is physically impossible. The second conjugate state represents a shock from the BP regime to the BP regime with comparable energy gain in the contracting layer and energy loss in the expanding layer. This too, we believe, is not a physical conjugate state although it is included in Table 2. We can focus primarily on the comparison

Table 2. *Comparison between YG and viscous theory (scaled values for $K = 1$)*

Case	Parameters $F_1; F_2$	Layer 1/2	Viscous model Δh	Viscous model $\Delta B\,(10^{-2})$	Yih and Guha Δh	Yih and Guha $\Delta B\,(10^{-2})$	M_{12}
a	$F_1 = 0.8$	1	0.1990	−0.11	0.1990	−0.066	1.003
	$F_2 = 0.1$	2	−0.2050	−0.028	−0.2045	0.015	
	$F_1 = 0.8$	1	—	—	0.6250	−1.2	—
	$F_2 = 0.1$	2	—	—	−0.876	19.0	
b	$F_1 = 0.1$	1	−0.4513	−0.44	−0.4312	0.080	−1.01
	$F_2 = 0.8$	2	0.8720	−1.9	0.8431	−2.0	
	$F_1 = 0.1$	1	—	—	−0.929	24.3	—
	$F_2 = 0.8$	2	—	—	1.370	−43.0	
c	$F_1 = 1.5$	1	0.611	−4.0	0.598	−3.6	1.004
	$F_2 = 2.0$	2	0.110	−0.27	0.101	−0.09	
d	$F_1 = 1.8$	1	0.681	−5.6	0.701	−7.2	1.09
	$F_2 = 1.5$	2	0.620	−4.6	0.575	−3.4	
e	$F_1 = 2.0$	1	0.421	−3.3	0.411	−2.9	0.971
	$F_2 = 1.5$	2	1.110	−11.0	1.11	−11.0	

between the first conjugate state and viscous model prediction.

For both case a and case b, the end states predicted by two theories are quite similar. Viscous theory predicts a slightly weaker contraction of the lower layer for case a and a slightly weaker contraction of the upper layer for case b. The Bernoulli losses are qualitatively different. Viscous theory predicts Bernoulli losses in both layers. YG's theory predicts a Bernoulli loss in the expanding layer and a small Bernoulli gain in the contracting layer.

In case a, $M_{12} > 1$, indicating that for an internal jump, YG's formulation underestimates the momentum transport from the upper layer to the lower layer. In case b, $M_{12} < -1$, indicating that for an internal drop, YG's formulation underestimates the momentum transport from the lower layer to the upper layer. The underestimate of momentum exchange is physically equivalent to mixing some momentum into the contracting layer, which might cause the Bernoulli value to increase in the contracting layer.

For case c, d, and e, both YG theory and viscous shock theory predict a unique conjugate state and Bernoulli losses in both layers. The momentum exchange rate (M_{12}) can be greater or less than unity.

YG's theory also predicts the existence of a cusp for strong external jumps. For $K = 1$, the cusp boundaries predicted by YG's theory is shown on Fig. 17. The cusp region predicted by YG is slightly larger than that predicted by viscous theory. The two tips are fairly close to each other. In Fig. 17, two points in the cusp, A and B, are taken as examples. For all three branches of

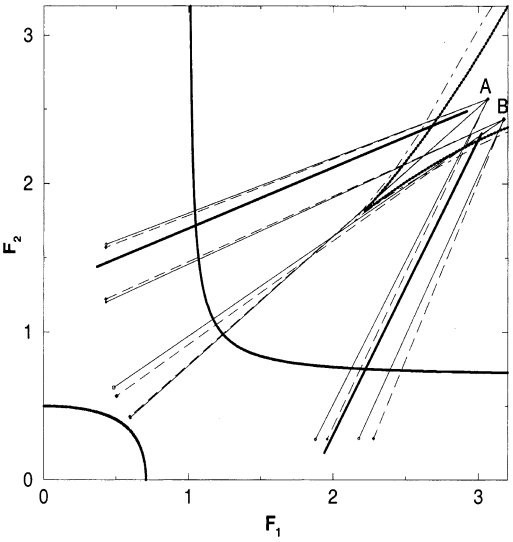

Fig. 17. Comparison of three shock models. Shock solutions from the viscous theory (solid line) and YG's theory (dashed line) for two points in the cusp region, i.e., point A ($F_1 = 4\cos 37.5°$, $F_2 = 4\sin 37.5°$) and point B ($F_1 = 4\cos 40°$, $F_2 = 4\sin 40°$). The lines connect between the initial and end-states. The two lines in bold represent shallow water model solutions with initial states in the vicinity of A and B.

solutions, the agreement between the two theories is satisfactory.

The 2 bold lines in Fig. 17 are centerline shock solutions from the shallow water model runs. The specified upstream flow states are A and B respectively. The upstream adjustment due to the underlying topographic forcing account for the departure of the pre-shock states from the specified upstream states. Nevertheless, a general agreement is obvious. The shallow water runs gives no middle branch solution.

In summary, at least for relatively weak shocks (shown in Table 2), there is a quantitative agreement between the YG and viscous shock theories in regard to the end-state prediction. In fact, to the lowest order (i.e., weak shock solutions), $M_{12} = 1$, and the two theories predict precisely the same end state.

There is no doubt that YG's formulation (i.e., two coupled third order algebraic equations) is much simpler than viscous shock theory (i.e., 2 coupled non-linear differential equations). The improved physical consistency of and the added information about shock existence and uniqueness from the viscous shock theory may make it more useful as a foundation for future research.

6. Summary

In this paper, we have developed a theory of shocks in two-layer flow with a passive layer above, using a pair of viscous model equations. It is convenient to describe the theory in two parts: the steepening condition and numerical solution.

The steepening condition arises mathematically in this problem from the need to find solutions which converge properly at upstream and downstream infinity. The three possible states of criticality of two layer flow (BB, BP and PP) are relevant to this issue. Critical curves, describing the condition of zero wave speed, mark the boundaries of these states. The discussion of linearized viscous "tail modes" leads to a set of rules concerning the critical curves that must be crossed during a shock transition. These rules in turn suggest a shock classification system. Shocks cannot start in BB nor end in PP. Monotonic shocks cannot both begin and end in BP. These rules eliminate 6 of the 9 possible transitions between the 3 states of criticality. The remaining 3 transitions are from BP to BB (i.e., an internal shock), from PP to BP (i.e., an external shock) or PP to BB (i.e., two-mode shock). The "two-mode shock" satisfies the steepening condition but can be ruled out on other grounds. The steepening condition can be extended, using the Total Momentum (TM) constraint, to prohibit pre-shock states in part of BP.

The steepening condition is a necessary but not sufficient condition for shock existence and, it does not specify uniqueness. For example, large regions of parameter space BP satisfy the steepening condition, but in fact, do not support shocks. Furthermore, some parts of PP have shocks with multiple end states. Therefore, to construct a useful pre-shock state regime diagram, it is necessary to subdivide both PP and BP with respect to shock existence and uniqueness using a series of numerical solutions to the viscous model equations. The final result is shown in Fig. 4.

Regime BP is divided into 3 regions: internal jumps and drops and a no-shock subregime (BP-n). Some pre-shock states in BP-n have no shock solutions because their TM curves do not enter BB. Other states in BP-n would give shocks that are so strong that they "overshoot" BB, ending up in BP again so that the steepening tendency is absent.

Regime PP is also divided into three regions. First is a large subregime (PP-1) composed of weak and moderate strength shocks of three types: lower layer, two-layer and upper layer jumps. Each pre-shock state in PP-1 has a unique end state. Second is a cusp-shaped region (PP-3) with strong shocks where each pre-shock state has three distinct end states, corresponding to lower layer, two-layer, and upper layer jumps. Topologically, the cusp is a folding over of the three shock type domains found in PP-1. We argue that the middle-branch, corresponding to two-layer jumps, is inaccessible. Third is PP-∞, where each pre-shock state has an infinity of end states. This subregime is inaccessible however, as it lies on the middle branch of PP-3.

The cusp in PP has several physical implications. It indicates that an equal distribution of dissipation between the two layers is mathematically possible but physically inaccessible. Thus, external jumps tend to concentrate their dissipation in one of the layers. It also allows a non-uniqueness in the final state of the jump and promotes hysteresis in time varying flows. In

practice, the concentration of dissipation and PV generation in the upper or lower layer becomes very sensitive to upstream shear. A striking consequence of the cusp character of strong external jumps is that even if the initial state is unsheared, the end state is so rapidly sheared that the conditions for an internal shock may then be nearly met. Thus, a strong external jump may be followed by an internal shock.

It is interesting that internal shocks must start with asymmetric flow and have a tendency to make a 2-layer flow more symmetric. On the other hand, external shocks can start with either symmetric or slightly asymmetric flow, but, always make a 2-layer flow more asymmetric.

The model equations give a mechanistic picture of how Bernoulli loss occurs in a shock. The viscous force in an ideal shock can be decomposed into two parts: normal viscous force and unbalanced viscous force (SS95). The normal viscous force can locally increase or decrease the Bernoulli constant but the sum of its contributions across a shock is zero. The unbalanced viscous force generated at the sloping interface always has the tendency to destroy energy and reduce the Bernoulli constant. For a weak shock, the unbalanced viscous force is only a small portion of the total viscous force. Therefore, the variation of Bernoulli function within a shock is much larger than the net Bernoulli loss after a shock. For a strong external shock, these two components are comparable. The Bernoulli curve drops strongly and only slightly recovers giving a large net Bernoulli loss. Bernoulli loss is strongly concentrated in the layer with the larger relative depth change.

An objective of this work is to evaluate how existing numerical shallow water models handle shocks. All five types of shocks found in the theory have been simulated as bow shocks by a time dependent shallow water model. Shocks forming on the lee side of the obstacle are not included in this comparison as it is much more difficult to control their pre-shock states. A reasonable agreement between viscous model solutions and shallow water simulations has been found with respect to shock existence, uniqueness and end state properties.

The predictions of YG theory approximately agree with viscous theory, but YG has two problems: no existence/uniqueness theorem and, due to a small error in the momentum exchange formulation, an unphysical Bernoulli rise in the contracting layer.

7. Acknowledgments

Christoph Schär kindly allowed us to use his shallow water code. The paper benefited from the recommendations of two reviewers. This research was supported by the National Science Foundation, Division of Atmospheric Sciences (ATM-9711076).

REFERENCES

Armi, L. 1986. The hydraulics of two flowing layers of different densities. *J. Fluid Mech.* **163**, 27–58.

Armi, L. and Williams, R. 1993. The hydraulics of a stratified fluid flowing through a contraction. *J. Fluid Mech.* **251**, 355–375.

Baines, P. G. and Davies, P. A. 1980. Laboratory studies of topographic effects in rotating and/or stratified fluids. *GARP Pub. Ser.* **23**, Orographic Effects in Planetary Flows, ICSU/WMO, pp. 233–299.

Baines, P. G. 1984. A unified description of two-layer flow over topography. *J. Fluid Mech.* **146**, 127–167.

Baines, P. G. 1995. *Topographic effects in stratified flows.* Cambridge University Press, 488 pp.

Benton, S. G. 1954. The occurrence of critical flow and hydraulic jumps in a multi-layered fluid system. *J. of Meteorol.* **11**, 139–150.

Chu, V. H. and Baddour, R. E. 1977. Surges, waves and mixing in 2-layer density stratified flow. *Proc. 17th Congr. Intl Assn Hydraul. Res.*, vol. **1**, 303–310.

Gilmore, R. 1981. *Catastrophe theory for scientists and engineers.* Wiley, New York, 666 pp.

Houghton, D. D. C. 1964. An example of interaction between finite-amplitude gravity waves. *J. Atmos. Sci.* **21**, 493–499.

Houghton, D. D. C. and Kasahara, A. 1968. Nonlinear shallow fluid flow over an isolated ridge. *Commun. Pure Apple. Maths* **21**, 1–23.

Houghton, D. D. C. and Isaacson, E. 1968. Mountain winds. *Studies in Num. Anal.* **2**, 21–52.

Jiang, Q. and Smith, R. B. 2000. V-wave, bow wave, and wakes in supercritical hydrostatic flow. *J. Fluid Mech.* **406**, 27–53.

Jiang, Q. and Smith, R. B. 2001. Ideal shocks in two layer flow, Part I: Under a rigid lid. *Tellus* **53B**, 129–145.

Klemp, J. B., Rotunno, R. and Skamarock, W. C. 1997. On the propagation on internal bores. *J. Fluid Mech.* **331**, 81–106.

Long, R. R. 1954. Some respects of the flow of stratified fluids (II). Experiments with a two-fluid system. *Tellus* **6**, 97–115.

Long, R. R. 1956. Solitary waves in the one and two fluids systems. *Tellus* **8**, 460–471.

Long, R. R. 1970. Blocking effects in flow over obstacles. *Tellus* **22**, 471–480.

Long, R. R. 1972. Finite amplitude disturbances in the flow of inviscid rotating and stratified fluids over obstacles. *Ann. Rev. Fluid Mech.* **4**, 69–92.

Mehrotra, S. C. 1973. Limitation on the existence of shock solutions in a two fluid system. *Tellus* **15**, 169–173.

Mehrotra, S. C. and Kelly, R. E. 1973. On the question of non-uniqueness of internal hydraulic jumps and drops on a two fluid system. *Tellus* **15**, 560–567.

Schär, C. and Smith, R. B. 1993. Shallow-water flow past an isolated topography. Part I: Vorticity production and wake formation. *J. Atmos. Sci.* **50**, 1373–1400.

Schär, C. and Smolarkiewicz, P. K. 1996. A synchronous and iterative flux-correction formalism for coupled transport equations. *J. Comput. Phys.* **128**, 101–120.

Smith, R. B. and Smith, D. F. 1995. Pseudoviscid wake formation by mountains in shallow water flow with a drifting vortex. *J. Atmos. Sci.* **52**, 436–454.

Wood, I. R. and Simpson, J. E. 1984. Jumps in layered miscible fluids. *J. Fluid Mech.* **140**, 329–342.

Yih, C. S. and Guha, C. R. 1955. Hydraulic jump in a fluid system of two layers. *Tellus* **7**, 358–366.